

Neural Modulation Alteration to Positive and Negative Emotions in Depressed Patients: Insights from fMRI Using Positive/Negative Emotion Atlas

Yu Feng¹, Weiming Zeng^{1*}, Yifan Xie¹, Hongyu Chen¹, Lei Wang¹, Yingying Wang¹, Hongjie Yan², Kaile Zhang³, Ran Tao³, Wai Ting Siok³, Nizhuan Wang^{3*}

1. Lab of Digital Image and Intelligent Computation, Shanghai Maritime University, Shanghai 201306, China
2. Department of Neurology, Affiliated Lianyungang Hospital of Xuzhou Medical University, Lianyungang 222002, China
3. Department of Chinese and Bilingual Studies, The Hong Kong Polytechnic University, Hong Kong, SAR, China

* Corresponding authors:

Weiming Zeng,

Email: zengwm86@163.com

Nizhuan Wang,

Email: wangnizhuan1120@gmail.com

Abstract:

Background: Although it has been noticed that depressed patients show differences in processing emotions, the precise neural modulation mechanisms of positive and negative emotions remain elusive. FMRI is a cutting-edge medical imaging technology renowned for its high spatial resolution and dynamic temporal information, making it particularly suitable for the neural dynamics of depression research.

Methods: To address this gap, our study firstly leveraged fMRI to delineate activated regions associated with positive and negative emotions in healthy individuals, resulting in the creation of positive emotion atlas (PEA) and negative emotion atlas (NEA). Subsequently, we examined neuroimaging changes in depression patients using these atlases and evaluated their diagnostic performance based on machine learning.

Results: Our findings demonstrate that the classification accuracy of depressed patients based on PEA and NEA exceeded 0.70, a notable improvement compared to the whole-brain atlases. Furthermore, ALFF analysis unveiled significant differences between depressed patients and healthy controls in eight functional clusters during the NEA, focusing on the left cuneus, cingulate gyrus, and superior parietal lobule. In contrast, the PEA revealed more pronounced differences across fifteen clusters, involving the right fusiform gyrus, parahippocampal gyrus, and inferior parietal lobule.

Limitations: Due to the limited sample size and subtypes of depressed patients, the efficacy may need further validation in future.

Conclusions: These findings emphasize the complex interplay between emotion modulation and depression, showcasing significant alterations in both PEA and NEA among depression patients. This research enhances our understanding of emotion modulation in depression, with implications for diagnosis and treatment evaluation.

Keywords:

fMRI; Positive Emotion; Negative Emotion; Depression; SVM; ALFF;

1 Introduction

Depression, also known as depressive disorder, is a serious mental illness characterized by elevated prevalence, frequent recurrence, significant suicide-related mortality, and a substantial disease burden (McIntyre et al., 2023). The core symptoms of depression include an increase in negative emotions and a lack of positive emotions (Chen et al., 2019). Patients with depression often exhibit pronounced negative emotions such as sadness, anxiety, irritability, and self-blame. Unlike negative emotions, positive emotions are generally beneficial; however, in patients with depression, positive emotions may exhibit complex features. In some cases, patients with depression may have a diminished response to positive emotions, making it challenging for them to experience feelings such as happiness and satisfaction (Kupferberg and Hasler, 2023). Conversely, in certain situations, patients with depression may exhibit intense positive emotional reactions; however, these positive emotions are often fleeting and quickly give way to a return to depression (Deng et al., 2022). Therefore, understanding the causes and healing mechanisms of depression has been the focus of research. Clinical practice primarily relies on drug treatment for depression, but about 30% of patients with depression do not respond well to medication (Shi et al., 2021). Moreover, the changes in brain regions and the treatment needs of patients with different subtypes, severities, and accompanying symptoms are highly heterogeneous. Traditional diagnosis and treatment methods struggle to accurately assess the condition of these patients.

In recent years, a plethora of neuroimaging modalities has surfaced to investigate the structure and function of the human brain, with fMRI standing out as a pivotal methodology. This technique adeptly captures fluctuations in blood oxygen level-dependent signals within the brain, offering insights into the activity states of various brain regions and their interrelationships (Wang et al., 2023). Given the temporal and spatial resolution of fMRI imaging, along with the recognition that abnormal manifestations of depression primarily arise from atypical activity and interactions within brain regions (Wen et al., 2024), more researchers are using fMRI to investigate depression-related phenomena. For instance, Sheline et al. (2010) employed fMRI to evaluate resting-state functional connectivity (RSFC) within cognitive control, default mode, and affective networks in individuals with depression. They found increased connectivity in all three networks, particularly with ipsilateral dorsomedial prefrontal cortex regions, compared to healthy controls. Seema and Shankapal (2018) examined differential brain activation patterns between depressed patients and healthy individuals during various music stimulation tasks using fMRI. Their results underscored significant activation within the anterior cingulate cortex, dorsolateral prefrontal cortex, and striatum in individuals with depression. Rubin-Falcone et al. (2020) employed fMRI to study the neural correlates of emotional reactivity and emotion regulation during the viewing of emotionally salient images as predictors of treatment outcomes with Cognitive Behavioral Therapy (CBT) for major depressive disorder (MDD). Their results indicated that the neural correlates of emotional reactivity might possess stronger predictive power for CBT outcomes. Keller et al. (2021), with fMRI, found that left ventrolateral prefrontal cortex (vlPFC) neurofeedback (NF) was associated with heightened bilateral frontal self-regulation and enhanced emotion regulation. After NF training in the left hemisphere, 75% of individuals with MDD reported successful application of learned strategies in daily life. Cosgrove et al. (2020) employed fMRI to explore the relationship between parents' emotion socialization practices and adolescent brain function during emotion processing. Negative parental verbalizations during conflict discussions were associated with increased thalamic activity in the emotion reactivity tasks and across several brain regions during the costly error condition of the Testing Emotional Attunement and Mutuality task. To date, researchers have predominantly focused on aberrant alterations in brain structure, functional connectivity (FC), and neural activity in individuals with depression (Gray

et al., 2020; Liu et al., 2020; Hare and Duman, 2020). However, few studies have delved into the distinctions of relevant brain regions in depressed patients, particularly concerning alterations in regions associated with positive and negative emotions as observed in neurotypical individuals. Moreover, there is a lack of comprehensive research elucidating the changes and underlying mechanisms in specific brain regions closely linked to positive and negative emotions in depressed patients.

In current studies, the analysis and diagnosis of brain disorders generally rely on the universal template, which provides a basic framework for disease research but lack specificity when dealing with specific diseases such as depression (Shusharina et al., 2023). Because depression has complex emotional changes and individual differences, generic templates often fail to capture the unique emotional changes of patients, resulting in unsatisfactory diagnostic efficacy. Therefore, there is a need for a depression-specific emotional template, which can accurately capture the subtle differences in patients' emotional changes (Park et al., 2023). At the same time, the accuracy of traditional Region of Interest (ROI) level templates in depression diagnosis was not high. In fMRI imaging, a voxel serves as the smallest unit of analysis, akin to a pixel in a two-dimensional image (Wang et al., 2018). The fMRI-derived images are partitioned into abstract 3D grids, with each unit termed a voxel (Blazejewska et al., 2019). Given the registration process conducted according to distinct brain region templates, an indefinite number of voxels populate a brain region, allowing voxel-level investigations to offer a more nuanced analysis and potentially deeper insights into depression (Yu et al., 2021). Despite their advantages, voxel-based fMRI analysis methods are susceptible to technical limitations such as image registration and spatial transformation, which may affect the accuracy and reliability of results (Viessmann and Polimeni, 2021). Therefore, this paper posits the Positive Emotion Atlas (PEA) and Negative Emotion Atlas (NEA) as solutions to overcome these challenges.

In summary, two key questions regarding the relationship between negative/positive emotion modulation and depression remain unresolved. Firstly, the precise delineation of PEA and NEA is lacking, despite their significant activation in normal individuals in response to positive and negative emotional picture stimulation, respectively. Secondly, it is imperative to investigate the changes that occur in depressed patients under the PEA and NEA and determine whether they differ from those in healthy controls. To bridge these gaps, this study used fMRI technology to elucidate the activation regions associated with positive and negative emotions in healthy controls at both brain region and voxel levels, constructing the PEA and NEA. Subsequently, a Support Vector Machine (SVM) classifier (Roy and Chakraborty, 2023) was trained to distinguish between depression patients and healthy controls based on the entire brain and the constructed PEA and NEA. To enhance classification performance, the Cost-Sensitive Learning (CSL) (Shao et al., 2024) strategy was integrated into the SVM classifier. Further analysis utilizing Amplitude of Low-Frequency Fluctuation (ALFF) (Zhang et al., 2023) was designed to reveal significant differences between depressed patients and healthy controls.

2 Materials and Methods

2.1 Data Acquisition

2.1.1 Positive/Negative Stimulus Task FMRI Dataset

Twenty-one participants (12 males, 9 females) with an average age of 23.65 ± 1.5 years were recruited. All participants had normal or corrected-to-normal visual acuity, were in good health with no history of mental or serious physical illness, and were right-handed. Prior to the experiment, participants were fully informed of the study procedures and provided written informed consent in accordance with the guidelines approved by the Institutional Review Board (IRB) of East China Normal University

(ECNU). This study adhered to ethical principles and guidelines.

The fMRI images were obtained during exposure to positive and negative emotional stimuli, followed by resting-state scans. Stimulus images were sourced from the International Affective Picture System (IAPS) (Branco et al., 2023), to ensure consistency and reliability. The experimental paradigm, as depicted in Fig. 1, involved alternating periods of rest and emotional stimulation: rest - positive - rest - negative - rest - positive - rest - negative - rest - positive - rest - negative - rest. A 20-second resting period preceded the formal experiment, allowing subjects to stabilize their emotions. Each formal experiment lasted 240 seconds and comprised six blocks of 40 seconds each, alternating between task states (positive/negative emotional picture stimuli) and rest periods. Subjects viewed positive or negative emotional stimuli for 20 seconds during task blocks, which were presented randomly from the picture library. During rest periods, subjects lay flat with their heads fixed and were instructed to refrain from active thought while fixating on a white cross against a black background.

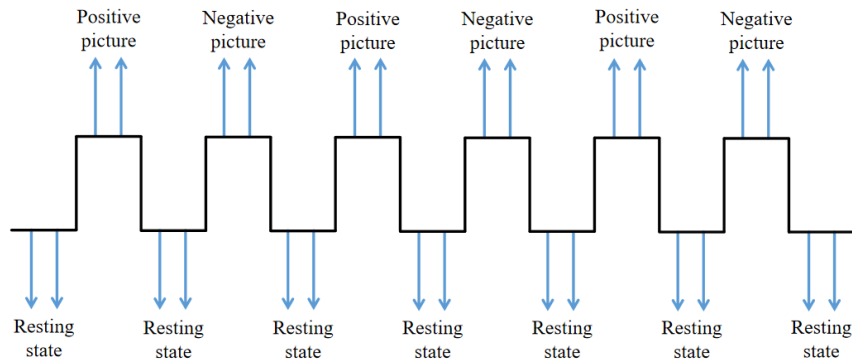


Figure 1. Schematic illustration of fMRI data acquisition paradigm (Zhao et al., 2023).

The fMRI data of 21 subjects were acquired at the Shanghai Key Laboratory of Magnetic Resonance at ECNU using a GE 3.0 Tesla MRI scanner. Imaging utilized a single-shot gradient echo planar imaging sequence comprising 33 slices, with a sensitivity acceleration factor of 2.0. Parameters included a repetition time (TR) of 2.0 seconds, a scan resolution of 64×64 , an in-slice resolution of $3 \text{ mm} \times 3 \text{ mm}$, a slice thickness of 4 mm, and a slice interval of 1 mm.

2.1.2 Resting-state Depression FMRI Dataset

The depression dataset used in this study was obtained from the public dataset OpenNeuro (<https://openneuro.org/>), with Accession Number DS002748 (Bezmaternykh et al., 2021). The original dataset included 51 depression patients and 21 healthy controls. However, one subject with dysthymia (sub-10), one with persistent mood disorder (sub-30), and one unannotated case (sub-34) were excluded from this study due to the limited number of subtypes. Additionally, during preprocessing, we identified problems with the data signal quality of sub-06, sub-15, and sub-60, so the data for these three subjects were also excluded. Ultimately, we selected resting-state fMRI data from 46 depression patients and 20 healthy controls from the original dataset, the details are shown in Table 1.

Table 1 Demographic and clinical characteristics of the groups involved in the study. M: males; F: females; SD: standard deviation; MADRS: Montgomery-Asberg depression rating scale; BDI: Beck depression inventory; ZSRDS: Zung self-rating depression scale.

Group	Sex	Age, Mean \pm SD	IQ, Mean \pm SD	MADRS, Mean \pm SD	BDI, Mean \pm SD	ZSRDS, Mean \pm SD
Healthy controls	6 M, 14 F	33.8 \pm 8.5	106.0 \pm 16.1	—	4.6 \pm 4.5	32.1 \pm 5.9
Depression patients	10 M, 36 F	33.1 \pm 9.5	103.7 \pm 14.6	26.7 \pm 4.4	20.7 \pm 10.0	46.4 \pm 7.0

standard deviation; MADRS: Montgomery-Asberg depression rating scale; BDI: Beck depression inventory; ZSRDS: Zung self-rating depression scale.

2.2 Positive/Negative Emotion Atlas Construction

The method for establishing the PEA and NEA is shown in Fig. 2. The process is divided into four steps. Firstly, data splitting and recombination are conducted, which involves timepoint segmentation based on the design of stimulus task blocks, resulting in 63 task blocks for both positive and negative emotional stimuli. Each task block comprises 5 time points of stimulus and resting-state image data. Secondly, data preprocessing is performed, and the preprocessed data are registered with the Brainnetome Atlas (Li et al., 2023) to obtain complete time series corresponding to signals from each brain region. Thirdly, feature collection involves normalization of the time series using Min-Max Normalization and calculating the mean, resulting in matrices of positive/negative emotion features for subsequent feature selection. Fourthly, feature selection is carried out using the Support Vector Machine recursive feature elimination (SVM-RFE) algorithm (Ranjan and Singh, 2023) to select brain regions significantly activated under positive and negative emotional stimuli, yielding characteristic ROIs. data preprocessing and feature collection are then performed on the voxels within characteristic ROIs, followed by another round of SVM-RFE algorithm to filter out characteristic sub-ROIs. Due to limitations in the extraction process, features in other brain regions might be missed. Therefore, this study selects external characteristic voxels with strong FC to the characteristic sub-ROIs, calculates their Pearson Correlation Coefficient, retains voxels with correlation greater than 0.95, and incorporates them to obtain the final PEA and NEA.

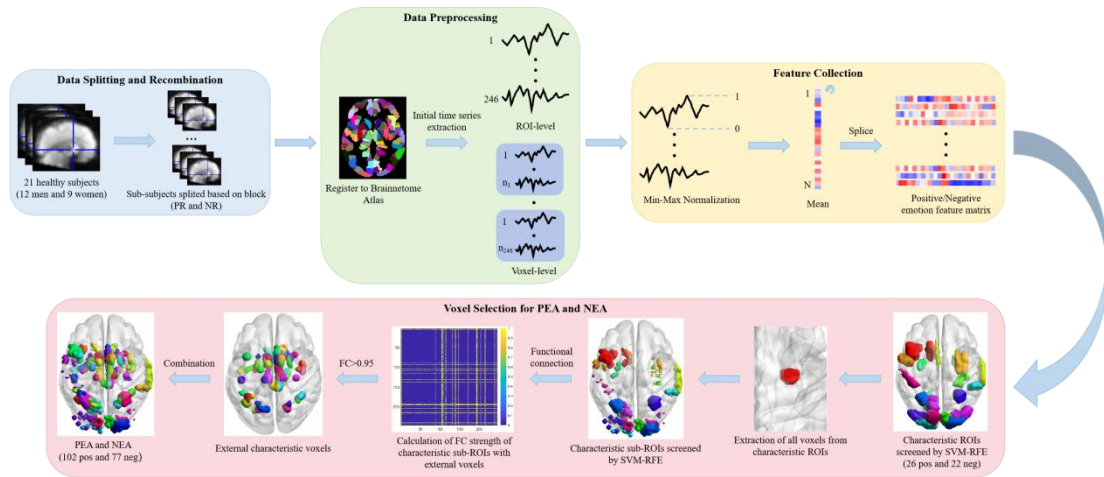


Figure 2. Flow chart of construction of PEA and NEA.

2.2.1 Data Splitting and Recombination

The data sets collected in this paper were divided into two categories. One type of data showed 20s of positive emotional stimulus pictures followed by 20s of white crosses on a black background, and the other type showed 20s of negative emotional stimulus pictures followed by 20s of white crosses on a black background. Because the BOLD signal of fMRI usually extends beyond the neural activity for 8-12s, and considering that few scholars have studied the difference between the stimulus state and the subsequent return to the baseline level, the data were split and reconstructed after the experiment in this paper. That is, in the time series of 40s, the data of 11-20s were extracted as the data of the positive/negative emotional stimulation state, and the data of 31-40s were extracted as the data of the recovery to the baseline state, so as to eliminate as much as possible the influence of human autonomous emotional fluctuations on this experiment. Since it takes 2s to scan the whole brain, for each 10-s block of tasks, five brain images will be extracted. After data extraction, the time series characteristics of the

Positive-Rest (PR) and Negative-Rest (NR) control groups were obtained.

Since this paper focuses on the detection of brain regions related to emotional function, it is desirable to eliminate the subject concept as much as possible. Therefore, the six task blocks of each subject in the formal experiment were extracted, and 21 subjects got 63 task blocks of positive and negative categories, respectively. A total of 10 brain images in the stimulus state and the resting state were obtained from each task block.

2.2.2 Data Preprocessing

Data preprocessing was performed on 63 task blocks with 20 brain images each. The main steps included slice timing, realign, spatial normalization, spatial smoothing and filtering, etc. The 33rd layer was used as the reference layer to correct the data of the septal scanning, and the image misalignment caused by the subject's head movement was adjusted. The images were standardized using the EPI template, the voxel size was set to $3 \times 3 \times 3 \text{ mm}^3$, FWHM= [4 mm, 4 mm, 4 mm], and the data at the frequency of 0.01Hz-0.1Hz were extracted. Finally, the pre-processed data were registered with Brainnetome Atlas to obtain the complete time series corresponding to the signals of each brain region for subsequent research.

2.2.3 Feature Collection

After data extraction and preprocessing, for different stimulus states and resting states of each task block, the data matrix was 5×246 , that is, 246 brain regions, and each brain region had data at 5 time points. Min-Max Normalization was performed on the data of each brain region in each task block, and then the average value of five time points was calculated. The 5×246 positive/negative emotional stimulus and resting-state matrices were converted into 1×246 matrices. Then, in the two types of comparison data, all the positive/negative emotional picture stimulation data and resting-state data will form two sets of data matrix 126×246 , of which 63 are positive/negative emotional stimulation states and 63 are the resting state after the corresponding emotional stimulation. For all the voxels in each brain region, the average activation value of each voxel in the positive/negative emotional stimulus state and the resting state was calculated after the Min-Max Normalization of the five time points of each voxel in the brain region. The overall process was similar to that of brain regions, and all features based on brain regions and voxels were finally obtained.

2.2.4 Voxel Selection for PEA and NEA

In order to find the characteristic ROIs and characteristic sub-ROIs significantly activated by positive and negative emotional stimuli, it is necessary to select all features and eliminate redundant information. In the analysis of brain region level, 246 brain regions were selected as the ROI, and the average activation value of brain regions under positive/negative emotional picture stimulation or resting state in a time series was used for feature selection. In the voxel-level analysis, all the voxels in a characteristic ROI were selected as the ROI, and the average activation value of the voxel in a time series was used as the feature for selecting. Positive emotional stimuli and resting state and negative emotional stimuli and resting state were used as two control groups. In this study, the SVM-RFE algorithm was used for feature selection of brain regions and voxels.

SVM is a generalized linear classifier, which is often used to solve binary classification problems (Liang et al., 2024). For the input independent variable x and label variable y , the objective function of SVM is as follows:

$$J = 1/2 \cdot \sum_{h=1}^N \sum_{k=1}^N y_h y_k \alpha_h \alpha_k (x_h \cdot x_k) - \sum_{k=1}^N \alpha_k \quad (1)$$

where, $0 \leq \alpha_k \leq C$ and $\sum_{k=1}^N \alpha_k y_k = 0$, there exists an optimal solution α_k for this objective function, then the decision function for input variable x is as follows:

$$D(x) = w \cdot x + b \quad (2)$$

$$W = \sum_{k=1}^N \alpha_k y_k x_k \text{ and } b = y_k - w \cdot x_k \quad (3)$$

SVM-RFE algorithm is a feature selection method combined with SVM, which uses the weight as the ranking criterion to backward delete features, and finally obtains the optimal feature subset (Azman et al., 2023). SVM-RFE feature selection algorithm has strong generalization ability and stable performance.

In order to make the results of feature selection more stable and robust, this study uses the SVM-RFE algorithm with 10-fold cross validation. Input two groups of training samples, $X_0 = [x_1, x_2, \dots, x_i, \dots, x_m]^T$ and $y = [y_1, y_2, \dots, y_i, \dots, y_m]^T$, each group of samples contains n features $s = [1, 2, \dots, n]$, For the set of all features, the feature with the smallest ranking coefficient is deleted in each iteration, until all the features are traversed, and the features that reach the maximum classification accuracy are retained as the selected features.

Each time the SVM model is trained, a weight vector W is generated:

$$W = \{w_1, w_2, \dots, w_i, \dots, w_n\} \quad (4)$$

Here w_i means the weight value of the i th ROI. Use W to compute the ranking criterion score for each round:

$$c_i = (w_i)^2, i = 1, 2, \dots, n \quad (5)$$

Due to the randomness of this ranking score, 10-fold cross validation is introduced to obtain the ten ranking criterion scores of the current feature, which are averaged to obtain the average ranking score as shown in the following equation:

$$a_i = \sum_{j=1}^{10} c_i^j / 10, i = 1, 2, \dots, n \quad (6)$$

where j is the j th fold in the 10-fold cross validation. The feature with the smallest average ranking coefficient in this round of 10-fold cross validation was deleted, and the final feature subset was obtained when the accuracy of the SVM trained classifier was no longer improved.

2.3 Identifying the Associated Regions in Depressed Patients under PEA and NEA

The method for detecting associated brain regions in depressed patients under PEA and NEA is shown in Fig. 3. In this study, classification validation was conducted separately across the Brainnetome Atlas template (246 brain regions), AAL template (90 brain regions) (Lee et al., 2024), Brodmann template (52 brain regions) (Trišins et al., 2024), and the PEA and NEA constructed within this study. When employing SVM classification with Radial Basis Function (RBF) (Li et al., 2023) based on CSL, we trained SVM using 10-fold cross validation to select appropriate parameter values from C (0.25, 0.5, 1, 2, 4) and γ (0.5, 1, 2, 4, 8, 15) to enhance classification accuracy. Incorporating CSL prioritizes avoiding higher-cost errors over merely improving accuracy, as misdiagnosing depression as healthy carries potentially greater consequences in medical diagnosis than misdiagnosing healthy as depressed. Additionally, ALFF analysis was performed on depression patients and healthy controls under PEA and

NEA, identifying clusters with significant differences under the two-sample t-test (FDR, $p < 0.01$) condition, followed by corresponding cognitive analysis.

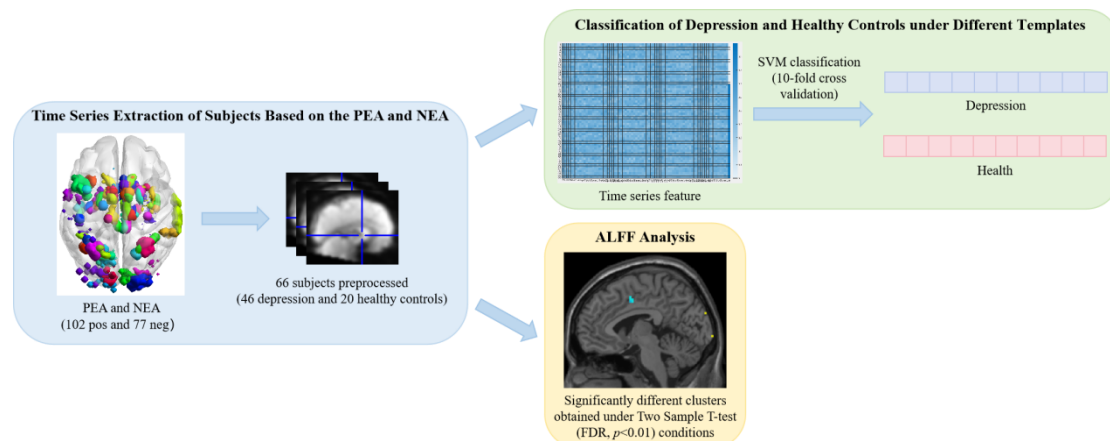


Figure 3. Flow chart of detection of associated brain regions in depressed patients under PEA and NEA.

3 Results

3.1 Determination of PEA and NEA in Normal Control

During characteristic ROIs selection, a total of 246 brain regions encompassing the entire brain served as the feature set. The average activation value of brain regions under positive/negative emotional picture stimulation or resting state in a time series was utilized as the feature. The SVM-RFE algorithm was applied for feature selection, yielding emotion-related characteristic ROIs for the PR and NR groups. To identify refined emotional characteristic sub-ROIs, the SVM-RFE algorithm was iteratively employed to filter all voxels within the characteristic ROIs, thereby achieving feature dimension reduction. Subsequently, after voxel dimension extraction, refined emotional characteristic sub-ROIs for the PR and NR groups were delineated.

3.1.1 Identified Positive Emotion-associated Activation Regions

Following the implementation of the Data Splitting and Recombination procedure, 63 task blocks were generated for both positive emotional picture stimulation and resting states. Each task block corresponded to a 1×246 feature vector. The feature vectors from positive emotional stimuli and resting states were combined to form a 126×246 feature matrix for selection. Subsequently, utilizing the SVM-RFE algorithm for feature selection, 26 positive emotion-activated characteristic ROIs were identified, spanning the frontal lobe, temporal lobe, parietal lobe, insular lobe, occipital lobe, and subcortical nucleus. These brain regions are detailed in Table 2, where their importance decreases gradually from top to bottom. Notably, the activated regions are predominantly concentrated in the parietal lobe, subcortical nucleus, temporal lobe, and occipital lobe.

Label ID	Gyrus	Hemisphere	MNI (X, Y, Z)
204	Lateral Occipital Cortex	LOcC_R_4_3	22, -97, 4
193	MedioVentral Occipital Cortex	MVOcC_L_5_3	-6, -94, 1
194	MedioVentral Occipital Cortex	MVOcC_R_5_3	8, -90, 12
131	Superior Parietal Lobule	SPL_L_5_4	-22, -47, 65
239	Thalamus	Tha_L_8_5	-16, -24, 6
88	Middle Temporal Gyrus	MTG_R_4_4	58, -16, -10

3	Superior Frontal Gyrus	SFG_L_7_2	-18, 24, 53
195	MedioVentral Occipital Cortex	MVOcC_L_5_4	-17, -60, -6
216	Hippocampus	Hipp_R_2_1	22, -12, -20
243	Thalamus	Tha_L_8_7	-12, -22, 13
146	Inferior Parietal Lobule	IPL_R_6_6	55, -26, 26
172	Insular Gyrus	INS_R_6_5	39, -7, 8
105	Fusiform Gyrus	FuG_L_3_2	-31, -64, -14
108	Fusiform Gyrus	FuG_R_3_3	43, -49, -19
93	Inferior Temporal Gyrus	ITG_L_7_3	-43, -2, -41
212	Amygdala	Amyg_R_2_1	19, -2, -19
140	Inferior Parietal Lobule	IPL_R_6_3	47, -35, 45
115	Parahippocampal Gyrus	PhG_L_6_4	-19, -12, -30
147	Precuneus	PCun_L_4_1	-5, -63, 51
156	Postcentral Gyrus	PoG_R_4_1	50, -14, 44
138	Inferior Parietal Lobule	IPL_R_6_2	39, -65, 44
21	Middle Frontal Gyrus	MFG_L_7_4	-41, 41, 16
214	Amygdala	Amyg_R_2_2	28, -3, -20
162	Postcentral Gyrus	PoG_R_4_4	20, -33, 69
57	Precentral Gyrus	PrG_L_6_3	-26, -25, 63
218	Hippocampus	Hipp_R_2_2	29, -27, -10

Table 2 Positive emotion-associated characteristic ROIs. Label ID is the characteristic ROI index in the Brainnetome Atlas. X, Y, Z represent the positions in MNI coordinates. L: left, R: right.

To refine the corresponding characteristic ROIs further, this experiment conducted quadratic feature selection in the voxel dimension to delineate more detailed characteristic sub-ROIs. Fig. 4 illustrates the comparison of the number of voxels in characteristic ROIs and characteristic sub-ROIs under the Brainnetome Atlas template. The results reveal a small number of retained voxels in each characteristic ROI, with some characteristic ROIs retaining only single-digit voxels exhibiting significant activation. This suggests that the fluctuations in activation value of these voxels under positive emotional stimulation significantly contribute to the activation of their respective characteristic ROIs.

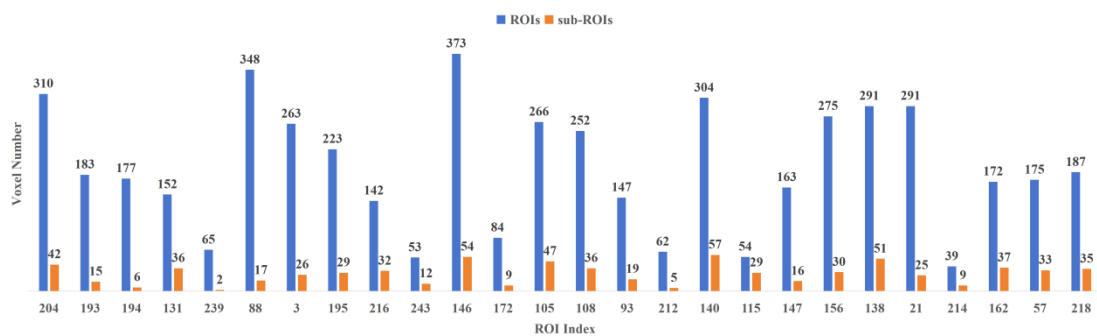


Figure 4. Comparison of the number of voxels in characteristic ROIs and characteristic sub-ROIs in the PR group.

The distribution of characteristic ROIs and characteristic sub-ROIs obtained by brain region and voxel feature selection in the human brain is shown in Fig. 5 and Fig. 6, respectively, and it can be seen that the characteristic ROIs after the secondary feature selection are significantly reduced. The characteristic sub-ROIs serve as the basis for the subsequent construction of PEA.

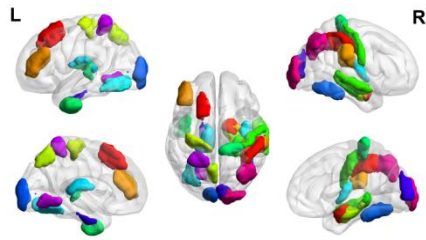


Figure 5. Voxel-based distribution of positive emotion-associated characteristic ROIs in the human brain.

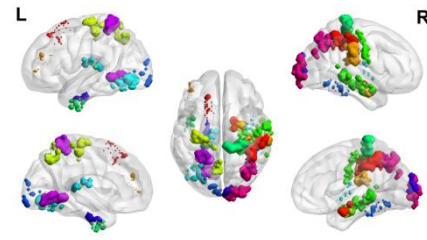


Figure 6. Voxel-based distribution of positive emotion-associated characteristic sub-ROIs in the human brain.

3.1.2 Identified Negative Emotion-associated Activation Regions

Following the implementation of the Data Splitting and Recombination procedure, 63 task blocks were generated for both negative emotional picture stimulation and resting states. Each task block corresponded to a 1*246 feature vector. The feature vectors from negative emotional stimuli and resting states were combined to form a 126*246 feature matrix for selection. Subsequently, utilizing the SVM-RFE algorithm for feature selection, 22 negative emotion-activated characteristic ROIs were identified, spanning the frontal lobe, temporal lobe, parietal lobe, insular lobe, limbic lobe, occipital lobe and subcortical nucleus. These brain regions are detailed in Table 3, where their importance decreases gradually from top to bottom. Notably, the activated regions are predominantly concentrated in occipital lobe, temporal lobe and parietal lobe.

Label ID	Gyrus	Hemisphere	MNI (X, Y, Z)
203	Lateral Occipital Cortex	LOcC_L_4_3	-18, -99, 2
204	Lateral Occipital Cortex	LOcC_R_4_3	22, -97, 4
167	Insular Gyrus	INS_L_6_3	-34, 18, 1
205	Lateral Occipital Cortex	LOcC_L_4_4	-30, -88, -12
194	MedioVentral Occipital Cortex	MVOcC_R_5_3	8, -90, 12
134	Superior Parietal Lobule	SPL_R_5_5	31, -54, 53
197	MedioVentral Occipital Cortex	MVOcC_L_5_5	-13, -68, 12
219	Basal Ganglia	BG_L_6_1	-12, 14, 0
230	Basal Ganglia	BG_R_6_6	29, -3, 1
104	Fusiform Gyrus	FuG_R_3_1	33, -15, -34
133	Superior Parietal Lobule	SPL_L_5_5	-27, -59, 54
151	Precuneus	PCun_L_4_3	-12, -67, 25
170	Insular Gyrus	INS_R_6_4	39, -2, -9
206	Lateral Occipital Cortex	LOcC_R_4_4	32, -85, -12
124	posterior Superior Temporal Sulcus	pSTS_R_2_2	57, -40, 12
76	Superior Temporal Gyrus	STG_R_6_4	66, -20, 6
207	Lateral Occipital Cortex	LOcC_L_2_1	-11, -88, 31
159	Postcentral Gyrus	PoG_L_4_3	-46, -30, 50
17	Middle Frontal Gyrus	MFG_L_7_2	-42, 13, 36
109	Parahippocampal Gyrus	PhG_L_6_1	-27, -7, -34
61	Precentral Gyrus	PrG_L_6_5	-52, 0, 8
177	Cingulate Gyrus	CG_L_7_2	-3, 8, 25

Table 3 Negative emotion-associated characteristic ROIs. Label ID is the characteristic ROI index in the Brainnetome Atlas. X, Y, Z represent the positions in MNI coordinates. L: left, R: right.

To refine the corresponding characteristic ROIs further, this experiment conducted quadratic feature selection in the voxel dimension to delineate more detailed characteristic sub-ROIs. Fig. 7 illustrates the comparison of the number of voxels in characteristic ROIs and characteristic sub-ROIs under the Brainnetome Atlas template. The results reveal a small number of retained voxels in each characteristic ROI, with some characteristic ROIs retaining only single-digit voxels exhibiting significant activation. This suggests that the fluctuations in activation value of these voxels under negative emotional stimulation significantly contribute to the activation of their respective characteristic ROIs.

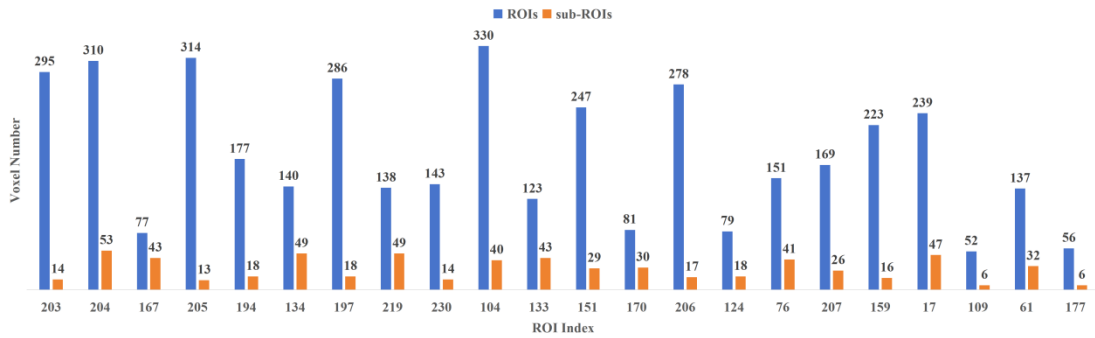


Figure 7. Comparison of the number of voxels in characteristic ROIs and characteristic sub-ROIs in the NR group.

The distribution of characteristic ROIs and characteristic sub-ROIs obtained by brain region and voxel feature selection in the human brain is shown in Fig. 8 and Fig. 9, respectively, and it can be seen that the characteristic ROIs after the secondary feature selection are significantly reduced. The characteristic sub-ROIs serve as the basis for the subsequent construction of NEA.

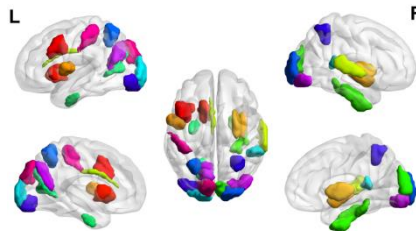


Figure 8. Voxel-based distribution of negative emotion-associated characteristic ROIs in the human brain.

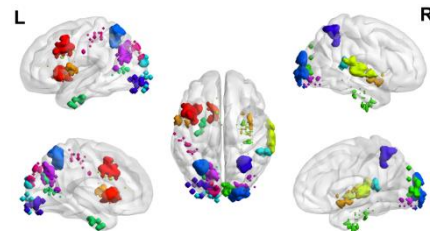


Figure 9. Voxel-based distribution of negative emotion-associated characteristic sub-ROIs in the human brain.

3.2 Results of Construction of PEA and NEA

The number of characteristic ROIs in PR group was 26, while the number of non-characteristic ROIs was 220, and these non-characteristic ROIs contained a total of 36398 voxels. The correlation coefficient between each voxel and the time series vector of 26 characteristic sub-ROIs was calculated. If the FC strength between each voxel and a characteristic sub-ROI was greater than 0.95, the voxel was retained. After FC analysis, a total of 776 voxels were retained and these voxels were distributed in 76 brain regions. The external characteristic voxels distribution extracted using FC strength is shown in Fig. 10. Combined with the above characteristic sub-ROIs, the final PEA of this paper was obtained, involving 102 brain regions, as shown in Fig. 11.

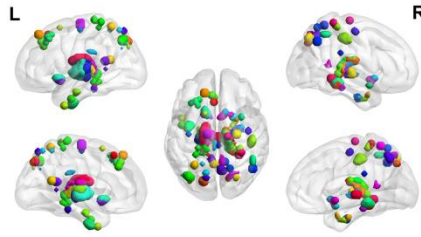


Figure 10. External characteristic voxels obtained by FC in the PR group.

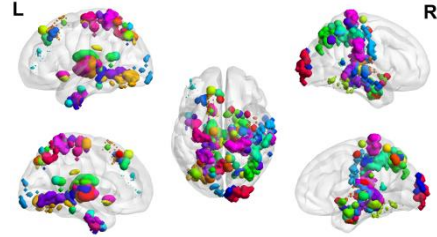


Figure 11. Demonstration of PEA.

The number of characteristic ROIs in NR group was 22, while the number of non-characteristic ROIs was 224, and these non-characteristic ROIs contained a total of 37400 voxels. The correlation coefficient between each voxel and the time series vector of 22 characteristic sub-ROIs was calculated. If the FC strength between each voxel and a characteristic sub-ROI was greater than 0.95, the voxel was retained. After FC analysis, a total of 715 voxels were retained and these voxels were distributed in 55 brain regions. The external characteristic voxels distribution extracted using FC strength is shown in Fig. 12. Combined with the above characteristic sub-ROIs, the final NEA of this paper was obtained, involving 77 brain regions, as shown in Fig. 13.

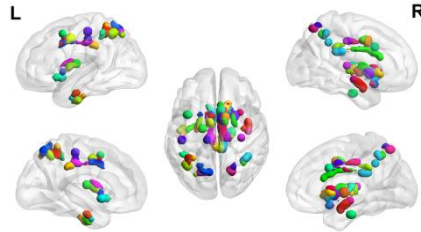


Figure 12. External characteristic voxels obtained by FC in the NR group.

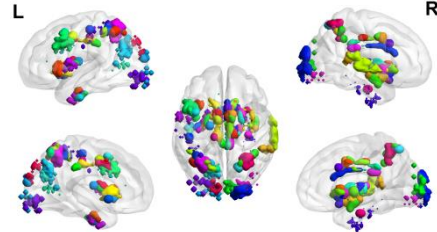


Figure 13. Demonstration of NEA.

To verify the PEA and NEA constructed in this paper, we used SVM classifiers based on RBF and CSL for classification verification, and used four quality measurement indicators of Accuracy, Precision, Recall and F-score to evaluate the effectiveness of templates.

In this experiment, we evaluated the PEA and NEA constructed in this paper, and extracted the time series of PR and NR using PEA, NEA, and Brainnetome Atlas templates. As shown in Fig. 14, the classification accuracy of PEA and NEA both exceeded 0.80. Especially when PEA and NEA were combined to extract features for classification, all performance indicators were better than those when using PEA or NEA alone.

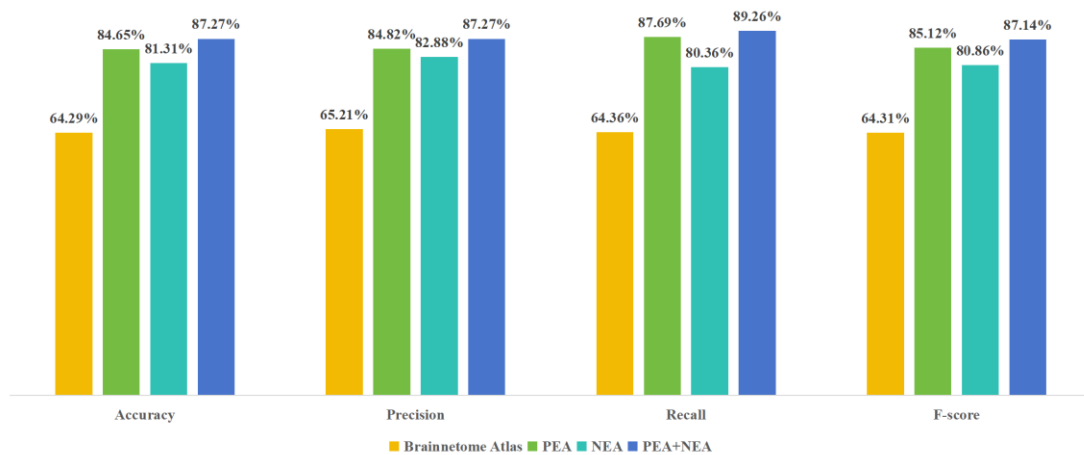


Figure 14 Classification Performance Comparison of various indicators of PR and NR under different templates on positive/negative stimulus task fMRI dataset.

In this experiment, we evaluated the application effects of PEA and NEA in patients with depression. We extracted time series from patients with depression and healthy controls using PEA, NEA, Brainnetome Atlas template, AAL template, and Brodmann template. As shown in Fig. 15, the classification accuracy of both PEA and NEA exceeds 0.70.

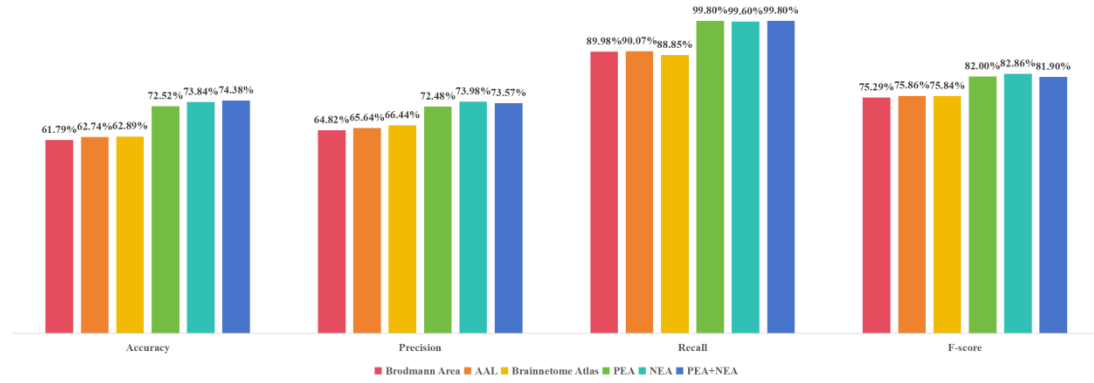


Figure 15. Classification Performance Comparison of various indicators between depression and healthy control groups under different templates on resting-state depression fMRI dataset.

3.3 Associated Regions in Depressed Patients under PEA and NEA

A two-sample t-test (FDR, $p < 0.01$) was conducted to compare the ALFF statistical brain maps between depression patients and healthy controls. Significant differences under the PEA revealed 15 clusters, as detailed in Table 4. Brain regions implicated included the right fusiform gyrus, parahippocampal gyrus, lingual gyrus, Sub-lobar, Extra-Nuclear, inferior parietal lobule, left parahippocampal gyrus, posterior cingulate, precuneus, precentral gyrus, thalamus, and corpus callosum. Notably, the left precentral gyrus exhibited a positive peak intensity of 2.83, while the peak intensities of other regions were negative, with the left posterior cingulate demonstrating the lowest intensity at -4.81.

Cluster	Number of voxels	Cluster Size (mm ³)	Peak MNI coordinate	Brain regions	Peak intensity
1	1	27	36, -48, -21	Right Cerebrum	-2.8682
				Temporal Lobe	
				Fusiform Gyrus	
2	1	27	39, -42, -21	Right Cerebrum	-2.905
				Temporal Lobe	
				Fusiform Gyrus	
3	2	54	15, -12, -21	Right Cerebrum	-3.4998
				Limbic Lobe	
				Left Cerebrum	
4	1	27	-15, -39, -9	Limbic Lobe	-2.7886
				Parahippocampa Gyrus	
				Right Cerebrum	
5	3	81	15, -33, -9	Limbic Lobe	-3.5011
				Parahippocampa Gyrus	
				lingual gyrus	

				Left Brainstem	
6	2	54	-15, -24, -6	Midbrain	-2.8383
				Thalamus	
				Medial Geniculum Body	
7	3	81	-15, -30, -3	Left Cerebrum	-3.5216
				Midbrain	
				Left Cerebrum	
8	1	27	-9, -48, 6	Limbic Lobe	-4.8121
				Posterior Cingulate	
				Right Cerebrum	
9	5	135	6, -42, 9	Sub-lobar	-4.3618
				Extra-Nuclear	
				Corpus Callosum	
				Left Cerebrum	
10	3	81	-6, -45, 15	Limbic Lobe	-3.8012
				Posterior Cingulate	
				Right Cerebrum	
11	1	27	57, -33, 36	Parietal Lobe	-2.7507
				Inferior Parietal Lobule	
				Right Cerebrum	
12	1	27	45, -54, 42	Parietal Lobe	-2.9547
				Inferior Parietal Lobule	
				Left Cerebrum	
13	1	27	-3, -57, 45	Parietal Lobe	-2.7553
				Precuneus	
				Left Cerebrum	
14	1	27	-9, -69, 51	Parietal Lobe	-2.9405
				Precuneus	
				Left Cerebrum	
15	1	27	-21, -21, 69	Frontal Lobe	2.8264
				Precentral Gyrus	

Table 4 Clusters with significant differences among depressed patients under the PEA. Peak intensity is the intensity of the maximum or minimum ALFF value in the statistically significant brain region, reflecting the extreme activity level of this brain region in the ALFF analysis.

A two-sample t-test (FDR, $p < 0.01$) was conducted on the data of depression patients and healthy controls, comparing the ALFF statistical brain maps between the two groups. Under the NEA, significant differences between the groups yielded 8 clusters, as detailed in Table 5. Implicated brain regions included the right superior temporal gyrus and middle temporal gyrus, as well as the left cuneus, middle frontal gyrus, cingulate gyrus, and superior parietal lobule. The peak intensity of the right superior temporal gyrus and middle temporal gyrus, as well as the left cuneus and middle frontal gyrus, were positive. Notably, the peak intensity of the right middle temporal gyrus was 3.11. Conversely, the peak intensity of the left cingulate gyrus, middle frontal gyrus, and superior parietal lobule was negative, with the peak intensity of the left superior parietal lobule recorded at -3.59.

Cluster	Number of voxels	Cluster Size (mm ³)	Peak MNI coordinate	Brain regions	Peak intensity
1	1	27	69, -30, 3	Right Cerebrum	2.9256
				Temporal Lobe	
				Middle Temporal Gyrus	
2	3	81	66, -24, 3	Right Cerebrum	3.1057
				Temporal Lobe	
				Superior Temporal Gyrus	
3	1	27	-12, -90, 30	Left Cerebrum	2.676
				Occipital Lobe	
				Cuneus	
4	1	27	-42, 21, 30	Left Cerebrum	2.7882
				Frontal Lobe	
				Middle Frontal Gyrus	
5	1	27	-3, -30, 42	Left Cerebrum	-2.7923
				Limbic Lobe	
				Cingulate Gyrus	
6	8	216	-6, -6, 48	Left Cerebrum	-3.2281
				Limbic Lobe	
				Cingulate Gyrus	
7	3	81	-51, 9, 42	Left Cerebrum	-3.1645
				Frontal Lobe	
				Middle Frontal Gyrus	
8	5	135	-9, -69, 57	Left Cerebrum	-3.5853
				Parietal Lobe	
				Superior Parietal Lobule	

Table 5 Clusters with significant differences among depressed patients under the NEA. Peak intensity is the intensity of the maximum or minimum ALFF value in the statistically significant brain region, reflecting the extreme activity level of this brain region in the ALFF analysis.

4 Discussion

4.1 Positive/Negative Emotion-associated Regions in Normal Control

The first three activated regions of positive emotion-associated characteristic ROIs were all occipital lobe regions, including the Lateral Occipital Cortex (LOcC_R_4_3), the MedioVentral Occipital Cortex (MVOcC_L_5_3, MVOcC_R_5_3). In addition to these three, the activated regions also included the MedioVentral Occipital Cortex (MVOcC_L_5_4). Because the experimental paradigm designed in this paper requires subjects to view pictures of different emotional stimuli, the activation of emotional regions is accompanied by the activation of visual regions. The largest proportion of the 26 regions activated was in the parietal lobe, accounting for seven of them, they were the Superior Parietal Lobule (SPL_L_5_4), the Inferior Parietal Lobule (IPL_R_6_2, IPL_R_6_3, IPL_R_6_6), the Precuneus (PCun_L_4_1) and the Postcentral Gyrus (PoG_R_4_1, PoG_R_4_4). They play an important role in attention and cognitive function. By regulating the brain's attention focus and understanding and analysis ability, they make the subjects have different responses to emotional stimulus pictures (Schröder et al., 2024). Moreover, they also participate in the regulation of emotional and social behaviors, helping the brain to identify

emotional expressions and participate in the understanding of social situations (Schreiner et al., 2019). Meanwhile, six subcortical nuclei were activated in response to positive emotion stimulation, including the Amygdala (Amyg_R_2_1, Amyg_R_2_2), the Hippocampus (Hipp_R_2_1, Hipp_R_2_2) and the Thalamus (Tha_L_8_5, Tha_L_8_7). Among them, the amygdala and hippocampus are considered to be related to emotion, and the amygdala is mostly involved in the generation and regulation of emotion. Barrett (2006) found that the amygdala is involved in predicting the threat or reward brought by emotional stimuli. While the hippocampus is associated with memory and emotional processing (Goode et al., 2020; McTeague et al., 2020), the data in this paper were extracted from subjects during viewing emotional stimulus pictures, and this process may trigger short-term memory of the picture content. The thalamus is the higher center of sensation, and its activation may be related to positive emotion production (Zhang et al., 2022). Furthermore, Fusiform Gyrus (FuG_L_3_2, FuG_R_3_3) in the temporal lobe region is an important part of the ventral visual system, which processes a large number of visual and visual-related signals and is sensitive to emotional stimulus pictures (Ternovoy et al., 2023). The Parahippocampal Gyrus (PhG_L_6_4), as the main cortical input to the hippocampus, has an important relationship with cognition and emotion (Li and Wang, 2021). Middle Temporal Gyrus (MTG_R_4_4) and Inferior Temporal Gyrus (ITG_L_7_3), which receive information from occipital lobe input, are more advanced regions of visual processing and also function as memory regions (Sun et al., 2022). In addition, three brain regions in the frontal lobe were significantly activated, namely the Superior Frontal Gyrus (SFG_L_7_2), Middle Frontal Gyrus (MFG_L_7_4) and Precentral Gyrus (PrG_L_6_3), which are often considered to be responsible for emotional regulation and decision-making, and can inhibit negative emotions such as anger, anxiety and fear produced by the amygdala (Gou et al., 2023). Only one brain region in the insular lobe was significantly activated, namely the Insular Gyrus (INS_R_6_5), which is often related to the production and representation of emotions (Zaki et al., 2012).

Four of the top five important activated regions for negative emotion-associated characteristic ROIs were occipital lobe regions, including Lateral Occipital Cortex (LOcC_L_4_3, LOcC_R_4_3, LOcC_L_4_4) and MedioVentral Occipital Cortex (MVOcC_R_5_3). In addition, three occipital lobe regions were included, namely Lateral Occipital Cortex (LOcC_R_4_4, LOcC_L_2_1) and MedioVentral Occipital Cortex (MVOcC_L_5_5). Similar to the positive emotion activation region, because the experimental paradigm designed in this paper requires subjects to view pictures of different emotional stimuli, the activation of emotional regions is accompanied by the activation of visual regions. Among the 22 activated regions, parietal lobe and temporal lobe regions accounted for the same proportion, and both accounted for four of them. Parietal lobe regions include the Superior Parietal Lobule (SPL_L_5_5, SPL_R_5_5), Precuneus (PCun_L_4_3), and Postcentral Gyrus (PoG_L_4_3), which are similar to the positive emotion activation region and will not be described in more detail here. Temporal lobe regions included the Superior Temporal Gyrus (STG_R_6_4), Fusiform Gyrus (FuG_R_3_1), Parahippocampal Gyrus (PhG_L_6_1) and posterior Superior Temporal Sulcus (pSTS_R_2_2). Similar to the positive emotion activation region, Watson et al. (2014) found that compared with the neutral expression, emotional expression induced more significant activation in the posterior superior temporal sulcus, and the higher the expression intensity, the greater the activation. At the same time, the Basal Ganglia (BG_L_6_1 and BG_R_6_6) in the subcortical nuclei region were significantly activated, with the former often considered related to emotion, and the latter related to the production mechanism of negative emotions (Sprenkelmeyer et al., 1998). Furthermore, the Middle Frontal Gyrus (MFG_L_7_2) and the Precentral Gyrus (PrG_L_6_5) of the frontal lobe regions were

also significantly activated, similar to the positive emotion activation region, which will not be described in more detail here. The Insular Gyrus (INS_L_6_3, INS_R_6_4) of the insular lobe region was also significantly activated, indicating that the activated regions of negative emotions were evenly and symmetrically distributed on both sides of the brain. In addition, only one brain region in the limbic lobe region was significantly activated, namely the Cingulate Gyrus (CG_L_7_2). Papez (1937) believed that emotional experience was mainly controlled by the cingulate gyrus and proposed the "Papez loop", and Kamali et al. (2023) updated the original Papez loop based on this concept.

4.2 Brain Regions in Depressed Patients under PEA and NEA

ALFF calculates the mean square root of the power spectrum of the signal in the low frequency range (0.01-0.08Hz), which is used to detect the regional intensity of spontaneous fluctuations in BOLD signal (Yue et al., 2023), and the variation in the regional intensity of the BOLD signal primarily reflects changes in blood flow and blood oxygenation levels in local brain regions, which are typically associated with neural activity, especially spontaneous or task-related neural activity. Therefore, the increase of ALFF may be a sign of excessive neural activity in brain regions, while the decrease of ALFF may indicate insufficient neural activity (Du et al., 2022). Previous studies have reported that machine learning models trained with ALFF features have good performance in identifying patients with depression and predicting antidepressant efficacy (Liu et al., 2019; Zhu et al., 2019).

Under the PEA, depressed patients in this study had significantly lower ALFF values than healthy controls in the right fusiform gyrus, which is generally considered to be related to the storage and recognition of faces. Depressed patients are prone to misunderstand other people's facial expressions, which may be related to weaker activation. Zhang et al. (2018) found that when the spontaneous brain activity of the fusiform gyrus is abnormal, patients with depression may have reduced recognition and memory of facial features, along with certain deviations in language understanding, leading them to have negative cognition in study and life. Additionally, Reynolds et al. (2014) found that the functional connectivity of the right fusiform gyrus in patients with mild cognitive impairment was abnormal, which may lead to memory defects, hallucinations and emotional disorders. Therefore, the dysfunction of the fusiform gyrus may be the neurophysiological basis for patients with depression being more prone to negative emotions. Lingual gyrus is located in the visual system and plays an important role in integrating visual information, introverted sensation and stimulation (Wang et al., 2019; Zhao et al., 2019). Consistent with the research of other scholars, the ALFF value of the right lingual gyrus in patients with depression in this study was also significantly lower than that of the healthy control group. Lee et al. (2016) found that the ALFF value of the bilateral lingual gyrus decreased in depressed patients with anxiety symptoms, and the gray matter connectivity of the right lingual gyrus changed abnormally in these patients. Jing et al. (2013) found that compared with the healthy control group, the ALFF/fALFF value of the left lingual gyrus of patients with depression was decreased. The inferior parietal lobule is involved in many functions such as attention, sensation and spatial information integration (Bečev et al., 2021). Wang et al. (2012) found that the ALFF value of the bilateral inferior parietal lobule in patients with first-episode depression decreased, with the significantly reduced region being the right inferior parietal lobule cortex. This is also consistent with the results of this study, which found that the ALFF value of the right inferior parietal lobule in patients with depression was significantly lower than that of the healthy control group. As the core brain region of the default mode network, the precuneus is related to many high-level cognitive functions and is responsible for self-related cognitive activities, such as collecting information and evaluating external emotional stimuli (Soldevila-Matías et al., 2022). Sendi

et al. (2021) conducted a brain network study on depression and found that when there was abnormal activity in the precuneus, patients would have cognitive disorders such as inattention, active negative thoughts, and negative emotional rumination. This study found that the ALFF value of the left precuneus in patients with depression was significantly lower than that of the healthy control group. This may be related to the clinical manifestation of repeated introspection in depressed patients. Thalamus is involved in the emergence of consciousness and is a neuronal transfer station for somatosensory conduction in the human body. It interacts with and influences the prefrontal-temporal lobe, prefrontal-amygdala, and prefrontal-basal ganglia, and participates in a series of cognitive and emotional processing processes (Barson et al., 2020). Because depression is characterized by emotional and cognitive impairments, many neuroimaging and histological studies have shown that dysfunction of the thalamus and its projection cortical targets are involved in both the pathology and physiology of depression (Spellman et al., 2020). In this study, there were significant differences in the left thalamus between patients with depression and healthy controls. We can speculate that there are functional and structural abnormalities in the thalamus in patients with depression, which cause symptoms such as loss of pleasure, attention, and memory decline. The parahippocampal gyrus can collect a variety of perceptual information, process and integrate it and then transmit it to the hippocampus, which plays a pivotal role in the cognitive processing of depression (Tartt et al., 2022). Lawrence et al. (2004) found that after patients with depression and healthy controls received different degrees of facial expression image stimulation such as fear, happiness and sadness, the activation response of the right parahippocampal gyrus to positive image stimulation in patients with depression was weakened, and the activation degree of the left parahippocampal gyrus was significantly positively correlated with the severity of depressive symptoms. This is partially consistent with the results of the present study, showing that the ALFF values of the parahippocampal gyrus were significantly lower in depressed patients than in healthy controls. The posterior cingulate is mainly involved in the regulation of emotions and self-awareness, while patients with depression often show emotional instability, reduced sense of self-worth, rumination and other symptoms, which are related to abnormal activity of the posterior cingulate cortex. Caetano et al. (2006) found structural changes with reduced posterior cingulate volume in patients with depression, which is in line with the results of this study that the ALFF value of the left posterior cingulate in patients with depression was significantly different from that in healthy controls. The corpus callosum is the most important nerve fiber bundle in the brain, connecting the coordination and integration of the left and right cerebral hemispheres (Valenti et al., 2020). Abnormal conduction of the corpus callosum can affect the emotional coordination, control, memory and attention of the left and right brains (Degraeve et al., 2023). Li et al. (2007) found that compared with the healthy control group, the fractional anisotropy (FA) values of the genu and body of the corpus callosum in patients with depression were significantly reduced, and the abnormal changes of Diffusion Tensor Imaging (DTI) only appeared in the genu and body of the corpus callosum. In this study, the ALFF value of the corpus callosum in patients with depression was significantly lower than that in healthy controls. There are few studies on the relationship between depression and the corpus callosum using fMRI technology, which can be further explored and improved in the future. The precentral gyrus is related to voluntary movement. Although this study showed that the ALFF value of the left precentral gyrus in patients with depression was significantly higher than that in the healthy control group, the patients with depression showed fewer limb movement abnormalities. Therefore, the relationship between the precentral gyrus and depression needs further research and analysis.

Under the NEA, the ALFF values in the right superior temporal gyrus and middle temporal gyrus of the depressed patients in this study were significantly higher than those of the healthy controls. The

superior temporal gyrus and middle temporal gyrus are not only related to mentalization ability, but also involved in the process of explaining and predicting individual behavioral ability based on autonomous beliefs, desires and emotions, as well as in the process of semantic processing and the regulation of emotional information and cognition (Li et al., 2023; Bo et al., 2024). Fan et al. (2013) found that ALFF activity in the right superior temporal gyrus was significantly enhanced in depressed patients with suicide attempts. Guo et al. (2016) found that the ALFF values of bilateral superior temporal gyrus and middle temporal gyrus were increased in patients with depression. Therefore, it can be speculated that the abnormalities of the superior temporal gyrus and middle temporal gyrus may lead to emotional disorders in patients with depression, and subsequently leading to negative cognition, depression, anxiety and other symptoms. The occipital lobe is involved in the coding and transmission of visual information in the cortex and the perception of various facial emotions (Zhang et al., 2022). The cuneus is a part of the occipital lobe and plays a core role in the neural network related to consciousness. The function of the cuneus may be related to the process of self-reflection, and it is involved in the extraction of visuospatial imagery and episodic memory. In this study, the ALFF value of the left cuneus of patients with depression was significantly higher than that of the healthy control group, Zhou et al. (2021) found a decrease in ALFF values in the left cuneus after 16 weeks of treatment with escitalopram and lithium in patients with bipolar II depression, which proved the results of this experiment in disguised form. Therefore, it can be speculated that cuneus dysfunction may lead to the preference of depressed patients for negative emotional information in episodic memory, and continuous attention to negative information may lead to the aggravation of depressive symptoms (Ternovoy et al., 2023). The cingulate gyrus plays a key role in cognitive and emotional information management, and it has extensive connections with brain regions that regulate emotion, the emotional valence of thoughts and autonomic nerves and visceral reflexes. Gong et al. (2020) found that the ALFF value of the posterior cingulate gyrus was significantly reduced in patients with MDD and bipolar disorder. In this study, it was found that the ALFF value of the left cingulate gyrus in patients with depression was significantly lower than that in healthy controls, which was consistent with the functional disorders of emotional instability and decreased decision-making ability in patients with depression. The activation of the superior parietal lobule is not only related to response inhibition, but it is also a key brain region for response inhibition control. The damage of its structure and function can cause the impairment of inhibitory control. Response inhibition is a cognitive process that removes inappropriate behavior attempts. It is an important component of executive function and plays an important role in making correct behavioral decisions to adapt to the requirements of environmental changes. In the present study, the ALFF value of the left superior parietal lobule was significantly lower in depressed patients than in healthy controls, and it can be speculated that depressed patients have weakened response inhibition function, which leads to increased impulsivity and increases the risk of suicide in depressed patients. The middle frontal gyrus is involved in cognitive processes of executive function and working memory, as well as emotional processing. In the present study, the ALFF value of the left middle frontal gyrus was significantly higher in depressed patients than in healthy controls in one part of the voxels, while it was opposite in the other part of the voxels. Cao et al. (2016) found that the ALFF value of the left middle frontal gyrus in depression patients without suicidal tendencies was significantly higher than that in healthy controls. Liu et al. (2012) found that patients with bipolar disorder had lower ALFF values in the left middle frontal gyrus during depression than healthy controls. Bremner et al. (1997) found that the metabolism of the middle frontal gyrus was reduced in normal people with induced depression. It has been suggested that the middle frontal gyrus may be a key site in the neuropathology of depression. These studies suggest that the dysfunction of the middle frontal

gyrus plays an important role in the induction of depressive emotion and the pathogenesis of depression.

5 Limitations

This study has some shortcomings. First, although fMRI technology has become quite mature in the field of medical imaging, it still faces challenges in accurately measuring emotional regulation because emotional and cognitive processes are complex and difficult to fully capture with a single imaging technique. While the PEA and NEA constructed in this paper contribute to understanding emotional regulation abnormalities in depression, they may overlook or miss certain subtle emotional differences in the construction process. Furthermore, due to a relatively small sample size, especially with the emotional dataset primarily consisting of graduate students, the generalizability of the research conclusions may be somewhat limited. Similarly, the sample size of the depression dataset may also be insufficient to comprehensively reflect various subtypes within the patient population. Lastly, this study is primarily based on cross-sectional data, lacking longitudinal data support, and is thus unable to verify whether the research findings remain stable or change over time. In summary, while this study provides a new perspective on the brain mechanisms of emotional regulation in depression, further research is still needed to overcome the aforementioned limitations.

6 Conclusion

This study, based on fMRI technology, proposes and constructs PEA and NEA based on voxel methodology, accurately identifying and locating brain regions and their voxels closely associated with positive/negative emotional responses. This atlas not only enhances the cognitive understanding of human emotional states but also, by comparing depression patients with healthy controls, reveals significant differences in neural mechanisms between the two groups, identifying key brain regions such as the cingulate gyrus, parahippocampal gyrus, and thalamus. With further validation and refinement, this atlas is expected to be utilized for early diagnosis of depression and the assessment of treatment efficacy.

Acknowledgements

This work was supported by the National Natural Science Foundation of China [grant number 31870979, 12304526].

References

- Azman, N. S., Samah, A. A., Lin, J. T., Majid, H. A., Shah, Z. A., Wen, N. H., & Howe, C. W. (2023). Support vector machine–Recursive feature elimination for feature selection on multi-omics lung cancer data. *Progress In Microbes & Molecular Biology*, 6(1), a0000327.
- Bremner, J. D., Innis, R. B., Salomon, R. M., Staib, L. H., Ng, C. K., Miller, H. L., ... & Charney, D. S. (1997). Positron emission tomography measurement of cerebral metabolic correlates of tryptophan depletion—induced depressive relapse. *Archives of General Psychiatry*, 54(4), 364-374.
- Barrett, L. F. (2006). Are emotions natural kinds?. *Perspectives on psychological science*, 1(1), 28-58.
- Blazejewska, A. I., Fischl, B., Wald, L. L., & Polimeni, J. R. (2019). Intracortical smoothing of small-voxel fMRI data can provide increased detection power without spatial resolution losses compared to conventional large-voxel fMRI data. *NeuroImage*, 189, 601-614.
- Barson, J. R., Mack, N. R., & Gao, W. J. (2020). The paraventricular nucleus of the thalamus is an

important node in the emotional processing network. *Frontiers in Behavioral Neuroscience*, 14, 598469.

Bezmaternykh, D. D., Melnikov, M. Y., Savelov, A. A., Kozlova, L. I., Petrovskiy, E. D., Natarova, K. A., & Shtark, M. B. (2021). Brain networks connectivity in mild to moderate depression: resting state fMRI study with implications to nonpharmacological treatment. *Neural Plasticity*, 2021.

Bečev, O., Mareček, R., Lamoš, M., Majchrowicz, B., Roman, R., & Brázdil, M. (2021). Inferior parietal lobule involved in representation of “what” in a delayed-action Libet task. *Consciousness and Cognition*, 93, 103149.

Branco, D., Gonçalves, Ó. F., & Badia, S. B. I. (2023). A systematic review of international affective picture system (iaps) around the world. *Sensors*, 23(8), 3866.

Bo, K., Kraynak, T. E., Kwon, M., Sun, M., Gianaros, P. J., & Wager, T. D. (2024). A systems identification approach using Bayes factors to deconstruct the brain bases of emotion regulation. *Nature Neuroscience*, 1-13.

Caetano, S. C., Kaur, S., Brambilla, P., Nicoletti, M., Hatch, J. P., Sassi, R. B., ... & Soares, J. C. (2006). Smaller cingulate volumes in unipolar depressed patients. *Biological psychiatry*, 59(8), 702-706.

Cao, J., Chen, X., Chen, J., Ai, M., Gan, Y., Wang, W., ... & Fang, W. (2016). Resting-state functional MRI of abnormal baseline brain activity in young depressed patients with and without suicidal behavior. *Journal of affective disorders*, 205, 252-263.

Chen, X., Zeng, W., Shi, Y., Deng, J., & Ma, Y. (2019). Intrinsic prior knowledge driven CICA FMRI data analysis for emotion recognition classification. *IEEE Access*, 7, 59944-59950.

Cosgrove, K. T., Kerr, K. L., Ratliff, E. L., Moore, A. J., Misaki, M., DeVille, D. C., ... & Morris, A. S. (2020). Effects of parent emotion socialization on the neurobiology underlying adolescent emotion processing: A multimethod fMRI study. *Research on child and adolescent psychopathology*, 1-13.

Deng, J., Chen, Y., Zeng, W., Luo, X., & Li, Y. (2022). Brain response of major depressive disorder patients to emotionally positive and negative music. *Journal of Molecular Neuroscience*, 72(10), 2094-2105.

Du, Y., Yang, W., Zhang, J., & Liu, J. (2022). Changes in ALFF and ReHo values in methamphetamine abstinent individuals based on the Harvard-Oxford atlas: A longitudinal resting-state fMRI study. *Addiction biology*, 27(1), e13080.

Degraeve, B., Sequeira, H., Mecheri, H., & Lenne, B. (2023). Corpus callosum damage to account for cognitive, affective, and social-cognitive dysfunctions in multiple sclerosis: A model of callosal disconnection syndrome?. *Multiple Sclerosis Journal*, 29(2), 160-168.

Fan, T., Wu, X., Yao, L., & Dong, J. (2013). Abnormal baseline brain activity in suicidal and non-suicidal patients with major depressive disorder. *Neuroscience letters*, 534, 35-40.

Guo D. L., Gao Y., Niu G. M. & Xie S. H. (2016). First-episode depression resting state of brain function low frequency amplitude research. *Magnetic resonance Imaging* (06),407-411.

Gong, J., Wang, J., Qiu, S., Chen, P., Luo, Z., Wang, J., ... & Wang, Y. (2020). Common and distinct patterns of intrinsic brain activity alterations in major depression and bipolar disorder: voxel-based meta-analysis. *Translational psychiatry*, 10(1), 353.

Gray, Jodie P., et al. "Multimodal abnormalities of brain structure and function in major depressive disorder: a meta-analysis of neuroimaging studies." *American Journal of Psychiatry* 177.5 (2020): 422-434.

Goode, T. D., Tanaka, K. Z., Sahay, A., & McHugh, T. J. (2020). An integrated index: engrams, place cells, and hippocampal memory. *Neuron*, 107(5), 805-820.

Gou, X. Y., Li, Y. X., Guo, L. X., Zhao, J., Zhong, D. L., Liu, X. B., R. J. (2023). The conscious

processing of emotion in depression disorder: a meta-analysis of neuroimaging studies. *Frontiers in Psychiatry*, 14, 1099426.

Hare, B. D., & Duman, R. S. (2020). Prefrontal cortex circuits in depression and anxiety: contribution of discrete neuronal populations and target regions. *Molecular psychiatry*, 25(11), 2742-2758.

Jing, B., Liu, C. H., Ma, X., Yan, H. G., Zhuo, Z. Z., Zhang, Y., ... & Wang, C. Y. (2013). Difference in amplitude of low-frequency fluctuation between currently depressed and remitted females with major depressive disorder. *Brain research*, 1540, 74-83.

Keller, M., Zweerings, J., Klasen, M., Zvyagintsev, M., Iglesias, J., Mendoza Quiñones, R., & Mathiak, K. (2021). fMRI neurofeedback-enhanced cognitive reappraisal training in depression: a double-blind comparison of left and right vLPFC regulation. *Frontiers in psychiatry*, 12, 715898.

Kupferberg, A., & Hasler, G. (2023). The social cost of depression: Investigating the impact of impaired social emotion regulation, social cognition, and interpersonal behavior on social functioning. *Journal of Affective Disorders Reports*, 100631.

Kamali, A., Milosavljevic, S., Gandhi, A., Lano, K. R., Shobeiri, P., Sherbaf, F. G., ... & Hasan, K. M. (2023). The cortico-limbo-thalamo-cortical circuits: an update to the original Papez circuit of the human limbic system. *Brain topography*, 36(3), 371-389.

Lawrence, N. S., Williams, A. M., Surguladze, S., Giampietro, V., Brammer, M. J., Andrew, C., ... & Phillips, M. L. (2004). Subcortical and ventral prefrontal cortical neural responses to facial expressions distinguish patients with bipolar disorder and major depression. *Biological psychiatry*, 55(6), 578-587.

Li J J, Kong X Q, Lin M F, Wang G H, Jiang X L, Li C Z... & Guo M. (2007). Diffusion Tensor Imaging Study of Corpus Callosum in Youth Major Depression. *J Clinical Radiology* (01),18-20.

Liu, C. H., Li, F., Li, S. F., Wang, Y. J., Tie, C. L., Wu, H. Y., ... & Wang, C. Y. (2012). Abnormal baseline brain activity in bipolar depression: a resting state functional magnetic resonance imaging study. *Psychiatry Research: Neuroimaging*, 203(2-3), 175-179.

Lee, Y. J., Kim, S., Gwak, A. R., Kim, S. J., Kang, S. G., Na, K. S., ... & Park, J. (2016). Decreased regional gray matter volume in suicide attempters compared to suicide non-attempters with major depressive disorders. *Comprehensive psychiatry*, 67, 59-65.

Liu, C. H., Tang, L. R., Gao, Y., Zhang, G. Z., Li, B., Li, M., ... & Wang, L. (2019). Resting-state map of neural signatures of vulnerability to depression relapse. *Journal of Affective Disorders*, 250, 371-379.

Liu, Yujie, et al. "Altered resting-state functional connectivity of multiple networks and disrupted correlation with executive function in major depressive disorder." *Frontiers in Neurology* 11 (2020): 272.

Li, X., & Wang, J. (2021). Abnormal neural activities in adults and youths with major depressive disorder during emotional processing: a meta-analysis. *Brain imaging and behavior*, 15, 1134-1154.

Li, W., Fan, L., Shi, W., Lu, Y., Li, J., Luo, N., ... & Jiang, T. (2023). Brainnetome atlas of preadolescent children based on anatomical connectivity profiles. *Cerebral Cortex*, 33(9), 5264-5275.

Li, W., Ye, S., Zhu, B., Hoffman, M., Zhou, J., & Yang, Q. (2023). Individual differences in harm-related moral values are associated with functional integration of large-scale brain networks of emotional regulation. *Journal of Neuropsychology*, 17(2), 335-350.

Li, Y., Wang, Z., & Dai, H. (2023). Improved Parkinsonian tremor quantification based on automatic label modification and SVM with RBF kernel. *Physiological Measurement*, 44(2), 025003.

Lee, D. J., Shin, D. H., Son, Y. H., Han, J. W., Oh, J. H., Kim, D. H., ... & Kam, T. E. (2024). Spectral Graph Neural Network-based Multi-atlas Brain Network Fusion for Major Depressive Disorder

Diagnosis. *IEEE Journal of Biomedical and Health Informatics*.

Liang, Y., Bo, K., Meyyappan, S., & Ding, M. (2024). Decoding fMRI data with support vector machines and deep neural networks. *Journal of Neuroscience Methods*, 401, 110004.

McTeague, L. M., Rosenberg, B. M., Lopez, J. W., Carreon, D. M., Huemer, J., Jiang, Y., ... & Etkin, A. (2020). Identification of common neural circuit disruptions in emotional processing across psychiatric disorders. *American Journal of Psychiatry*, 177(5), 411-421.

Ma, T., Ji, Y. Y., Yan, L. F., Lin, J. J., Li, Z. Y., Wang, W., ... & Cui, G. B. (2022). Gray matter volume abnormality in chronic pain patients with depressive symptoms: A systemic review and meta-analysis of voxel-based morphometry studies. *Frontiers in Neuroscience*, 16, 826759.

McIntyre, R. S., Alsuwaidan, M., Baune, B. T., Berk, M., Demyttenaere, K., Goldberg, J. F., ... & Maj, M. (2023). Treatment-resistant depression: definition, prevalence, detection, management, and investigational interventions. *World Psychiatry*, 22(3), 394-412.

Papez, J. W. (1937). A proposed mechanism of emotion. *Archives of Neurology & Psychiatry*, 38(4), 725-743.

Park, D., Lim, S., Choi, Y., & Oh, H. (2023). Depression Emotion Multi-Label Classification Using Everytime Platform with DSM-5 Diagnostic Criteria. *IEEE Access*, 11: 89093-89106.

Reynolds, S., Carrey, N., Jaworska, N., Langevin, L. M., Yang, X. R., & MacMaster, F. P. (2014). Cortical thickness in youth with major depressive disorder. *BMC psychiatry*, 14, 1-8.

Rubin-Falcone, H., Weber, J., Kishon, R., Ochsner, K., Delaparte, L., Doré, B., ... & Miller, J. M. (2020). Neural predictors and effects of cognitive behavioral therapy for depression: the role of emotional reactivity and regulation. *Psychological medicine*, 50(1), 146-160.

Ranjan, A., & Singh, V. P. (2023). Affirmative and negative sentence detection in the brain using svm-rfe and rotation forest: an fmri study. *SN Computer Science*, 4(4), 332.

Roy, A., & Chakraborty, S. (2023). Support vector machine in structural reliability analysis: A review. *Reliability Engineering & System Safety*, 233, 109126.

Sprengelmeyer, R., Rausch, M., Eysel, U. T., & Przuntek, H. (1998). Neural structures associated with recognition of facial expressions of basic emotions. *Proceedings of the Royal Society of London. Series B: Biological Sciences*, 265(1409), 1927-1931.

Sheline, Y. I., Price, J. L., Yan, Z., & Mintun, M. A. (2010). Resting-state functional MRI in depression unmasks increased connectivity between networks via the dorsal nexus. *Proceedings of the National Academy of Sciences*, 107(24), 11020-11025.

Seema, P. D., & Shankapal, P. (2018, March). A Comparative Audio Stimulus-fMRI study of Major Depressive Disorder (MDD) and Never Depressed (ND) Subjects. In 2018 IEEE International Conference on Electronics, Computing and Communication Technologies (CONECCT) (pp. 1-5). IEEE.

Schreiner, M. W., Klimes-Dougan, B., & Cullen, K. R. (2019). Neural correlates of suicidality in adolescents with major depression: resting-state functional connectivity of the precuneus and posterior cingulate cortex. *Suicide and Life-Threatening Behavior*, 49(3), 899-913.

Spellman, T., & Liston, C. (2020). Toward circuit mechanisms of pathophysiology in depression. *American Journal of Psychiatry*, 177(5), 381-390.

Sendi, M. S., Zendeihrouh, E., Sui, J., Fu, Z., Zhi, D., Lv, L., ... & Calhoun, V. (2021). Aberrant dynamic functional connectivity of default mode network predicts symptom severity in major depressive disorder. *Brain Connect*, 10.

Shi X, Yu D S & Lv D S.(2021). Advances in resting-state functional magnetic resonance imaging in treatment-resistant depression. *Inner Mongolia medical journal* (01), 31-33. Doi: 10.16096 / j.carol

carroll nki nmgyxzz. 2021.53.01.010.

Soldevila-Matías, P., Albajes-Eizagirre, A., Radua, J., García-Martí, G., Rubio, J. M., Tordesillas-Gutierrez, D., ... & Sanjuán, J. (2022). Precuneus and insular hypoactivation during cognitive processing in first-episode psychosis: Systematic review and meta-analysis of fMRI studies. *Revista de psiquiatria y salud mental*, 15(2), 101-116.

Sun, J. F., Chen, L. M., He, J. K., Wang, Z., Guo, C. L., Ma, Y., ... & Xu, F. Q. (2022). A comparative study of regional homogeneity of resting-state fMRI between the early-onset and late-onset recurrent depression in adults. *Frontiers in psychology*, 13, 849847.

Shusharina, N., Yukhnenko, D., Botman, S., Sapunov, V., Savinov, V., Kamyshov, G., ... & Voznyuk, I. (2023). Modern methods of diagnostics and treatment of neurodegenerative diseases and depression. *Diagnostics*, 13(3), 573.

Shao, H., Xu, Q., Yang, Z., Wen, P., Peifeng, G., & Huang, Q. (2024). Weighted roc curve in cost space: Extending auc to cost-sensitive learning. *Advances in Neural Information Processing Systems*, 36.

Schröder, J., Meller, T., Evermann, U., Pfarr, J. K., & Nenadić, I. (2024). Multi-modal morphometric association study of subclinical depressive symptoms using voxel-based morphometry, cortical thickness, and diffusion tensor imaging (DTI). *Journal of Affective Disorders*, 351, 755-764.

Tartt, A. N., Mariani, M. B., Hen, R., Mann, J. J., & Boldrini, M. (2022). Dysregulation of adult hippocampal neuroplasticity in major depression: pathogenesis and therapeutic implications. *Molecular psychiatry*, 27(6), 2689-2699.

Ternovoy, S., Ustyuzhanin, D., Shariya, M., Beliaevskaia, A., Roldan-Valadez, E., Shishorin, R., ... & Volel, B. (2023). Recognition of Facial Emotion Expressions in Patients with Depressive Disorders: A Functional MRI Study. *Tomography*, 9(2), 529-540.

Trišins, M., Zdanovskis, N., Platkājis, A., Šneidere, K., Kostiks, A., Karelis, G., & Stepens, A. (2024). Brodmann Areas, V1 Atlas and Cognitive Impairment: Assessing Cortical Thickness for Cognitive Impairment Diagnostics. *Medicina*, 60(4), 587.

Valenti, M., Pino, M. C., Mazza, M., Panzarino, G., Di Paolantonio, C., & Verrotti, A. (2020). Abnormal structural and functional connectivity of the corpus callosum in autism spectrum disorders: A review. *Review Journal of Autism and Developmental Disorders*, 7, 46-62.

Viessmann, O., & Polimeni, J. R. (2021). High-resolution fMRI at 7 Tesla: challenges, promises and recent developments for individual-focused fMRI studies. *Current opinion in behavioral sciences*, 40, 96-104.

Wang, N., Wu, H., Xu, M., Yang, Y., Chang, C., Zeng, W., & Yan, H. (2018). Occupational functional plasticity revealed by brain entropy: A resting-state fMRI study of seafarers. *Human brain mapping*, 39(7), 2997-3004.

Wang, L., Dai, W., Su, Y., Wang, G., Tan, Y., Z., ... & Si, T. (2012). Amplitude of low-frequency oscillations in first-episode, treatment-naive patients with major depressive disorder: a resting-state functional MRI study. *PloS one*, 7(10), e48658.

Watson, R., Latinus, M., Noguchi, T., Garrod, O., Crabbe, F., & Belin, P. (2014). Crossmodal adaptation in right posterior superior temporal sulcus during face–voice emotional integration. *Journal of Neuroscience*, 34(20), 6813-6821.

Wang, M., Cui, J., Liu, Y., Zhou, Y., Wang, H., Wang, Y., ... & Yu, Y. (2019). Structural and functional abnormalities of vision-related brain regions in cirrhotic patients: a MRI study. *Neuroradiology*, 61, 695-702.

Wang, L., Du, T., Zhao, L., Shi, Y., & Zeng, W. (2023). Research on the lateralization of brain

functional complexity in mild cognitive impairment-Alzheimer's disease progression based on multiscale lateralized brain entropy. *Biomedical Signal Processing and Control*, 86, 105216.

Wen, J., Antoniadis, M., Yang, Z., Hwang, G., Skampardoni, I., Wang, R., & Davatzikos, C. (2024). Dimensional Neuroimaging Endophenotypes: Neurobiological Representations of Disease Heterogeneity Through Machine Learning. *arXiv preprint arXiv:2401.09517*.

Yu, Q., Cai, Z., Li, C., Xiong, Y., Yang, Y., He, S., ... & Wang, N. (2021). A novel spectrum contrast mapping method for functional magnetic resonance imaging data analysis. *Frontiers in Human Neuroscience*, 15, 739668.

Yue, J., Zhao, N., Qiao, Y., Feng, Z. J., Hu, Y. S., Ge, Q., ... & Zang, Y. F. (2023). Higher reliability and validity of Wavelet-ALFF of resting-state fMRI: From multicenter database and application to rTMS modulation. *Human Brain Map*, 44(3), 1105-1117.

Zaki, J., Davis, J. I., & Ochsner, K. N. (2012). Overlap activity in anterior insula during interoception and emotional experience. *Neuroimage*, 62(1), 493-499.

Zhang, F. F., Peng, W., Sweeney, J. A., Jia, Z. Y., & Gong, Q. Y. (2018). Brain structure alterations in depression: Psychoradiological evidence. *CNS neuroscience & therapeutics*, 24(11), 994-1003.

Zhu, Y., Qi, S., Zhang, B., He, D., Teng, Y., Hu, J., & Wei, X. (2019). Connectome-based biomarkers predict subclinical depression and identify abnormal brain connections with the lateral habenula and thalamus. *Frontiers in psychiatry*, 10, 371.

Zhao, R., Zhang, X., Fei, N., Zhu, Y., Sun, J., Liu, P., ... & Qin, W. (2019). Decreased cortical and subcortical response to inhibition control after sleep deprivation. *Brain imaging and behavior*, 13, 638-650.

Zhou, J., Ma, X., Li, C., Liao, A., Yang, Z., Ren, H., ... & Chen, X. (2021). Frequency-specific changes in the fractional amplitude of the low-frequency fluctuations in the default mode network in medication-free patients with bipolar II depression: a longitudinal functional MRI study. *Frontiers in Psychiatry*, 11, 574819.

Zhang, Y., Zhang, Y., Ai, H., Van Dam, N. T., Qian, L., Hou, G., & Xu, P. (2022). Microstructural deficits of the thalamus in major depressive disorder. *Brain communications*, 4(5), fcac236.

Zhang, S., Tang, C., & Guan, C. (2022). Visual-to-EEG cross-modal knowledge distillation for continuous emotion recognition. *Pattern Recognition*, 130, 108833.

Zhang, J., Liu, D. Q., Qian, S., Qu, X., Zhang, P., Ding, N., & Zang, Y. F. (2023). The neural correlates of amplitude of low-frequency fluctuation: a multimodal resting-state MEG and fMRI-EEG study. *Cerebral Cortex*, 33(4), 1119-1129.

Zhao, W., Makowski, C., Hagler, D. J., Garavan, H. P., Thompson, W. K., Greene, D. J., ... & Dale, A. M. (2023). Task fMRI paradigms may capture more behaviorally relevant information than resting-state functional connectivity. *NeuroImage*, 270, 119946.